DIRECT SEM OBSERVATIONS AND MECHANISMS OF FATIGUE CRACK GROWTH

M. Jono and A. Sugeta
Department of Mechanical Engineering, Osaka University, Suita, Japan

ABSTRACT

Direct observations of growing fatigue cracks under cyclic loadings were made by a high-resolution, field emission type scanning electron microscope equipped with a specially designed servo-hydraulic fatigue loading system on both grain oriented and randomly oriented 3% silicon irons and fatigue crack growth mechanisms were investigated. Moreover, microscopic parameters which control the fatigue crack growth behaviors under both constant and variable amplitude loadings were discussed.

1. INTRODUCTION

The study of fatigue crack growth mechanisms is important for substantial understanding and accurate estimation of fatigue crack growth behavior. A considerable amount of microscopical approaches has been made to identify detailed mechanisms [1]-[3]. However, the majority of them has been based on post growth observations.

In the early work, one of the present authors and others have designed fatigue loading facilities operating in a scanning electron microscope (SEM) to realize such an approach, and have conducted fatigue crack growth tests on a grain oriented 3% silicon iron to elucidate the mechanism of Mode I crack growth at relatively high stress intensity regime [4],[5].

In this paper, results of direct observations of growing fatigue cracks at the relatively low growth rate regime on the same material were summarized, and correlation between crack growth rate and crack growth mode was discussed. Moreover, a micro-computer aided image sampling system and image processing technique were newly developed and controlling microscopic parameters were investigated for fatigue crack growth under both constant and variable amplitude loadings. In addition, the effects of grain orientation and grain boundary on crack growth behaviors were discussed by using a randomly oriented conventional 3% silicon iron.

2. EXPERIMENTAL PROCEDURE AND TEST MATERIALS

Fatigue crack growth tests were performed on the stage of SEM using a specially designed servo-hydraulic testing system under pulsating tensile loadings at frequency of 0.1 - 0.5 Hz. Schematic illustration of fatigue testing apparatus and block diagram of fatigue testing system are shown in Figs.1 and 2, respectively. The servo-hydraulic fatigue loading facility operating in an SEM is controlled by a micro-computer(NEC PC9801-VM2). The computer image processing and data sampling systems are composed of a micro-computer (NEC PC9801, memory capacity is 4 Mbytes) and a high-speed direct memory access (DMA) type A/D converter(ELMEC EC-2390). The secondary electron signal of the SEM was directly transferred to the main memory of the micro-computer through DMA type A/D converter with digitizing rate of 5 μsec per point to make it possible to sample the successive ten flames of SEM image data under fatigue loading of 0.1 Hz. The sampling cycle was found to not always synchronize with the scanning signal of the SEM , so the restructure of SEM images from the continuously sampled secondary electron signal data was made by detecting the starting points of sweep and scanning signals of the SEM.

The load-point displacement was detected with a beam type extensometer and the bulk closure behavior of fatigue crack was monitored throughout testing by computer aided unloading elastic compliance technique [6].

The materials investigated are grain oriented 3% silicon iron (grain diameter: 2 - 4 mm) and randomly oriented 3% silicon iron (50 - 100 μm). The dimensions and crystallographical orientation of test specimen of grain oriented material are shown in Fig.3. The loading axis is perpendicular to the rolling

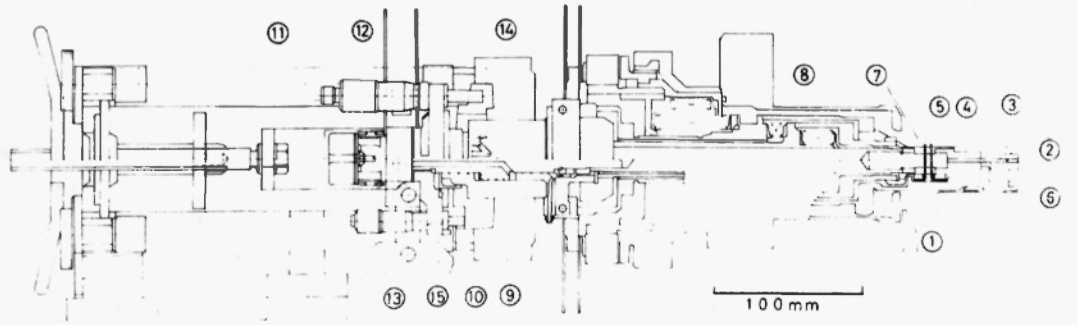

① Field-emission SEM ② Specimen ③ Specimen grip connected to cylinder
④ Specimen grip connected to piston ⑤ Load cell ⑥ Specimen stage
⑦ Airlock chamber ⑧ Flange ⑨ Piston ⑩ Cylinder
⑪ Servo-valve ⑫ Fine micrometer ⑬ Coarse micrometer ⑭ Ringed beam
⑮ Flexible joint ⑯ Blancing spring

Fig.1 Fatigue testing machine in Field-emission type SEM.

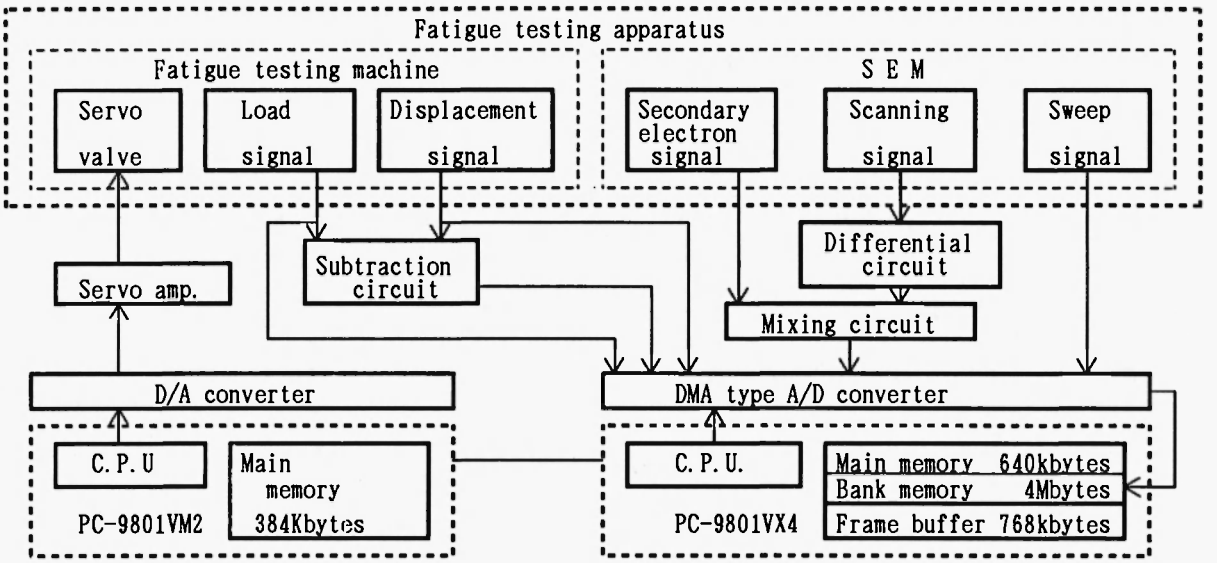

Fig.2 Block diagram of fatigue testing system.

direction, [100]. When the specimen is stressed, among four slip directions only two slip directions, $[1\bar{1}1]$ and $[11\bar{1}]$, lying in the plane of the sheet can operate and since other slip directions, [111] and $[\bar{1}11]$, in the plane perpendicular to the sheet do not operate, nearly perfect plane strain deformation results even right on the specimen surfaces [4],[7],[8]. The specimens were mechanically polished with emery papers and finally electro-polished. Fine magnesium oxides were scattered on a surface of the specimen as location markers and then the surface was gold coated to enhance resolution in SEM images.

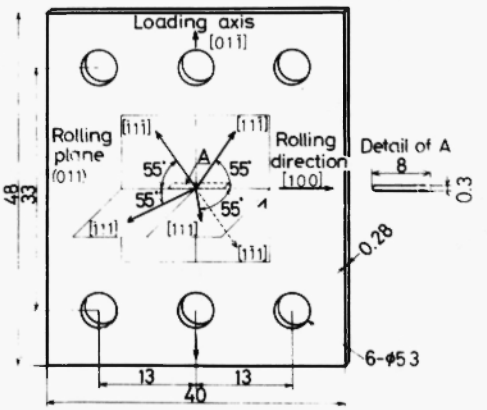

Fig.3 Dimensions and crystallographic orientation of test specimen.

3. EXPERIMENTAL RESULTS AND DISCUSSION

3.1 Fatigue Crack Growth Direction and Growth Mechanism

Figure 4 shows typical photographs of crack growth behaviors taken at different stress intensity levels [9]. When the applied K was so high that two preferential slip directions operated to almost identical extent simultaneously, fatigue crack grew in near Mode I through the striation mechanisms, as illustrated in Fig.4(d). However at low K levels, normally one slip direction operated more intensely relative to the other, which resulted in the mixed growth Mode I and II, and after certain period alternatively the other became more activated, so that crack advanced microscopically in zigzag manner as shown in Figs.4(a) and (b). Further, since the period while each slip direction

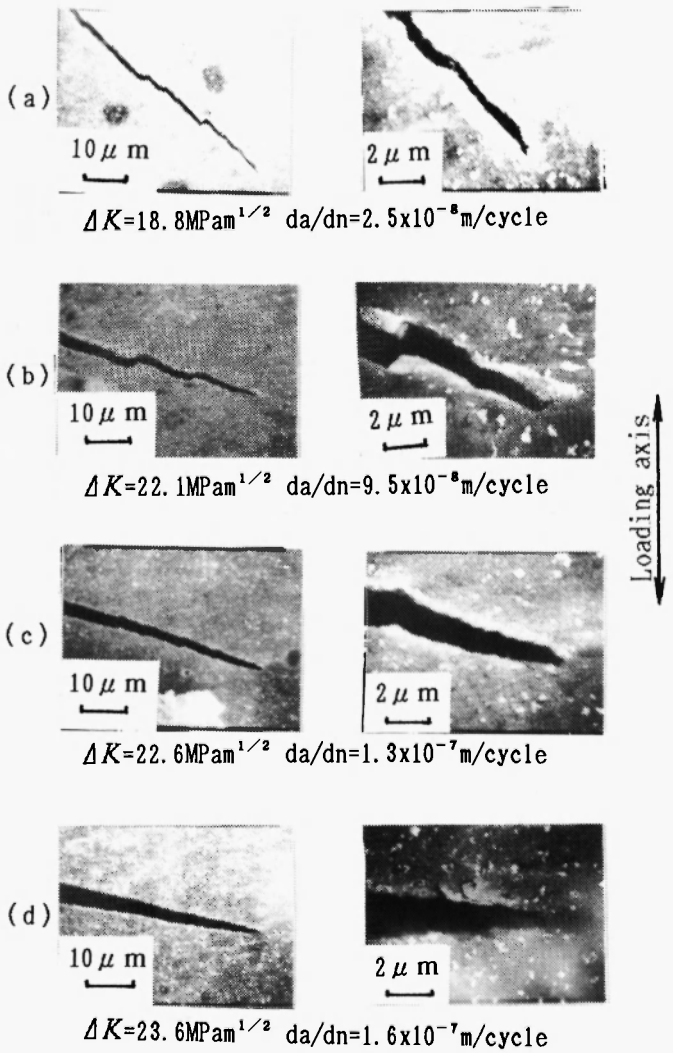

Fig.4 Examples of direct observation of growing fatigue cracks.

operated more actively varied depending on K levels, eventually macroscopic growth direction deviated from the ideal Mode I growth, depending on K levels or corresponding growth rates. It is worthy of note that except for the high growth rate region above about 10^{-7} m/cycle, fatigue cracks normally grow in the mixed Mode of I and II even in macroscopical sense under pure tensile loadings, as supposed from the results of measurements of crack opening displacement by Davidson and Lankford[10].

The microscopic crack growth direction defined as the direction over the distance of 2 - 3 μm behind the crack tip, θmic, was found to strongly depend on crack growth rate, (da/dn)mic, as shown in Fig.5. At the growth rate below 10^{-8} m/cycle crack growth direction coincided with the preferential slip direction of the material, while Mode I crack was realized at the growth rate above about 2×10^{-7} m/cycle. In the region between these growth rates microscopic crack growth direction angle decreased with increase of crack growth rate.

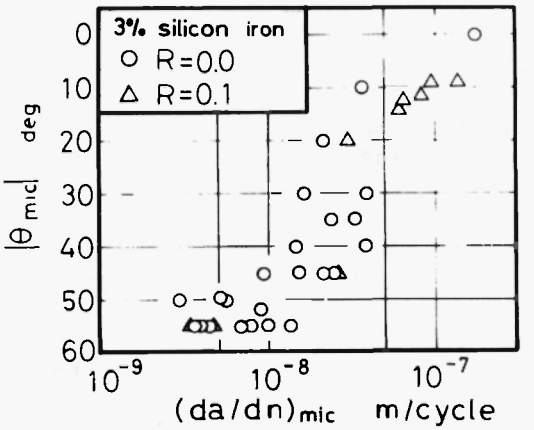

Fig.5 Relationship between crack rate and crack inclination angle.

From the above mentioned observations of growing fatigue cracks, a model of fatigue crack growth is proposed in Fig.6. Fatigue crack is normally supposed to propagate in zigzag manner along two slip directions of the material as explained in Figs.6(a) to (d), and the macroscopic crack growth direction is determined by a ratio of the growth increment along one slip direction to the other. And since the ratio is dependent on the stress intensity levels, inclination of macroscopic crack growth direction decreases with increase of the stress intensity level as shown in Fig.6(e).

3.2 Crack Tip Opening Displacement and Crack Growth Rate

Crack tip opening displacement (CTOD) is well understood as a good parameter to correlate with crack growth rate. For the Mode I crack it is easy to define the CTOD on the photographs of fatigue cracks [4]. However, since fatigue crack is usually growing in mixed Mode I and II, as mentioned in the previous section, and has rounded crack tip shape, it becomes rather difficult to define the CTOD. So in this study, crack opening displacement (COD) as well

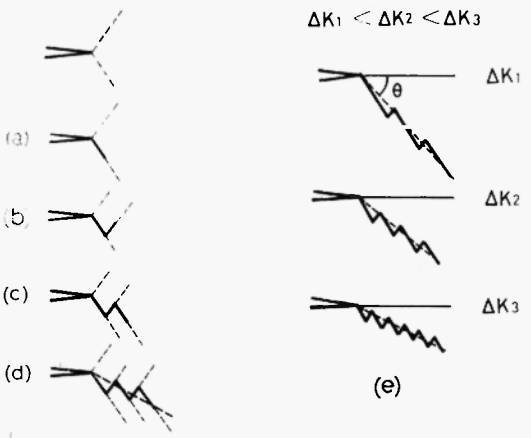

Fig.6 Fatigue crack growth model at low stress intensity level.

as CTOD is tried to be measured with the aid of image processing techniques as follows.

The flow chart of fatigue crack analysis is shown in Fig.7. Firstly, crack region is detected by thresholding as to the brightness of secondary electron signal of the SEM image. Figure 8 shows a sample of brightness distribution indicating that the region with low brightness value corresponds to fatigue crack and that with high brightness to magnesium oxides, and mid-region shows the test specimen surface. Since the brightness distribution of crack overlaped with that of the test specimen surface, it was difficult to separate crack region and specimen surface region, clearly. So, crack region was recognized as the largest one among the regions detected by thresholding using the optimum threshold value. The SEM image processed by thresholding is shown in Fig.9. Secondly, crack region was divided to small regions at crack deflection points and principal axis of inertia of each region was calculated. Center line of fatigue crack was obtained by connecting the each principal axis of inertia. Crack opening displacement(COD) is defined as the opening displacement in perpendicular direction to crack center line as shown in Fig.10. Figures 11(a) and (b) show examples of COD measurements where are shown fatigue cracks in the

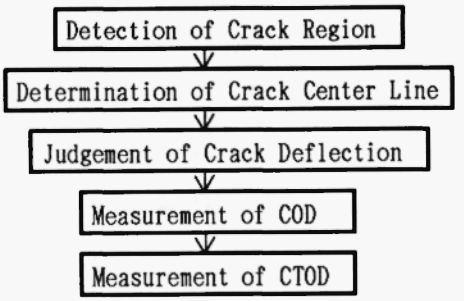

Fig.7 Flow chart of crack analysis procedure.

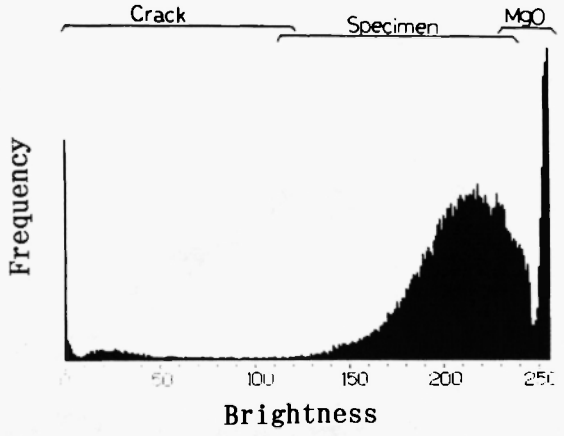

Fig.8 Brightness distribution of SEM photograph.

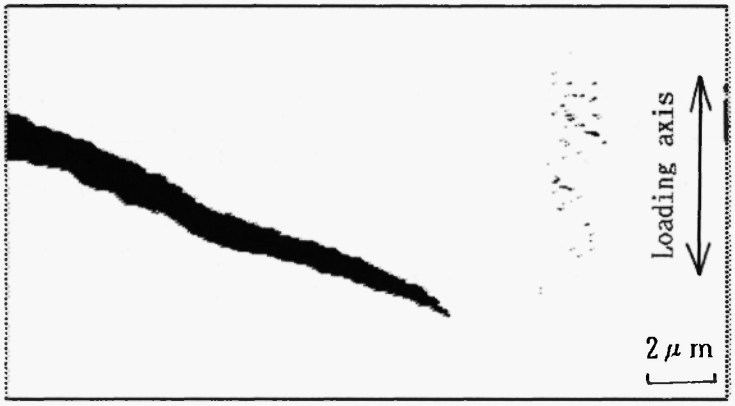

Fig.9 SEM image processed by thresholding.

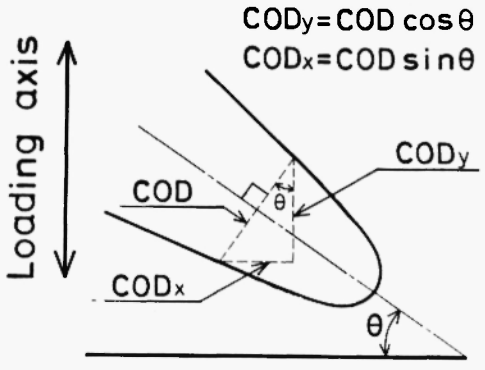

Fig.10 Definition of crack opening displacement.

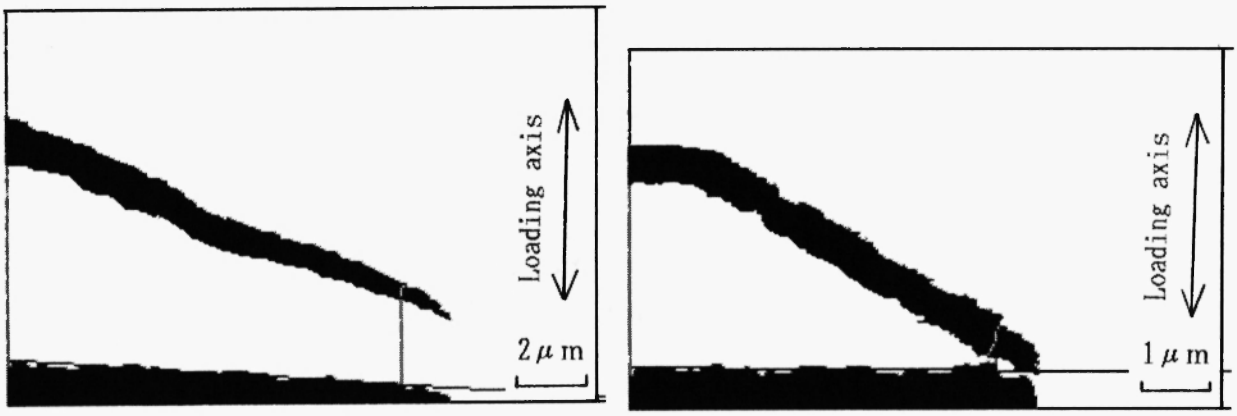

(a) CTOD = 15 (pixel) = 0.51 (μm)
θmic (CTOD) = 21.3 (degree)

(b) CTOD = 30 (pixel) = 1.02 (μm)
θmic (CTOD) = 31.1 (degree)

Fig.11 Examples of crack opening displacement(COD) measurement.

middle, and the measured COD values are shown in the bottom of each figure, respectively. The COD gradually decreased with approaching to the crack tip and the abrupt change of COD near crack tip was observed. Crack tip opening displacement(CTOD) was defined as the location where the abrupt change of COD occurred.

Figure 12 shows the relationship between the perpendicular component of microscopic growth rate to the loading axis and the vertical (tensile) component

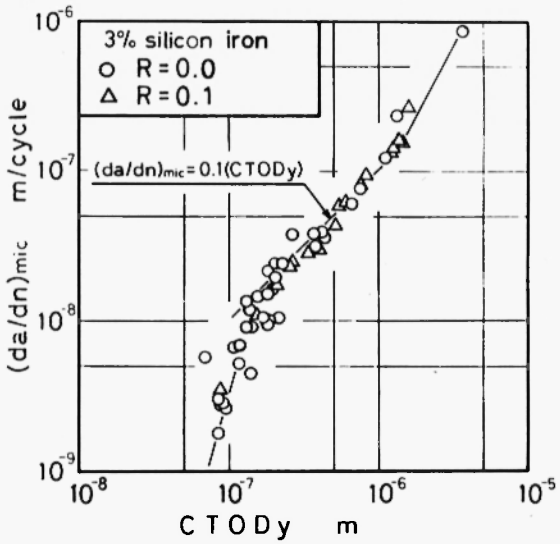

Fig.12 Relationship between CTODy and crack growth rate.

of CTOD, CTODy [11]. Here some points of CTOD and θmic were measured on the SEM photographs and the other measured by using above mentioned image processing technique. It was found that there existed a good correlation between crack growth rate and CTOD, and the ratio of growth increment to CTOD in the region of growth rate from 10^{-8} to 2×10^{-7} m/cycle was about one-tenth, which means that the tensile component of CTOD plays an important role for the growth behavior even in the mixed mode fatigue cracks. However, the ratio of one-tenth is small compared to that of Mode I crack where 0.7 was implied from a geometrical consideration or 0.5 - 0.6 was obtained in measurement [4]. The reason why the ratio is small in mixed mode crack is not clear, but it may be suggested that the Mode II component enhances the rewelding of crack tip in vacuum environment. Moreover, in the region of crack growth rate below 10^{-8} m/cycle considerable decrease of the ratio of crack growth increment to CTOD was found with decrease of crack growth rate in Fig.12.

Figure 13 shows the relationships between CTODy and the stress intensity range, ΔK, and the effective stress intensity range, ΔK_{eff}, where different symbols denote the different specimens. In the region above the CTOD of 10^{-8} m, where crack growth rate is larger than 10^{-7} m/cycle as known from Fig.12 and Mode I is dominant, CTOD was found proportional to square of the stress intensity range as supposed from fracture mechanics concept, while the inclination of the curve became steep in the region below the CTOD of 10^{-8} m and different relationships were obtained for different specimens, which resulted in different microscopic crack growth rates at the identical stress intensity level depending on the specimens, probably because of the difference in microscopic characteristics of the material such as microstructure and cyclic hardened or softened states.

3.3 Two Step Variable Amplitude Loading and Crack Growth Behavior

Figure 14 shows the macroscopic crack path, microscopic crack growth direction and variation of microscopic crack growth rate with crack growth increment

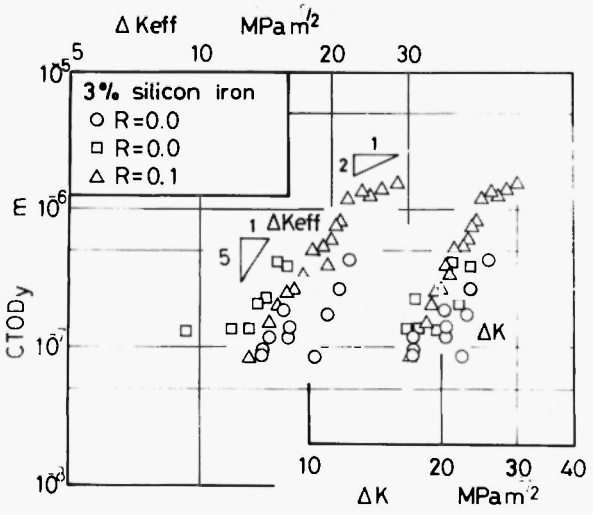

Fig.13 Relationship between ΔK and CTODy, ΔK_{eff} and CTODy.

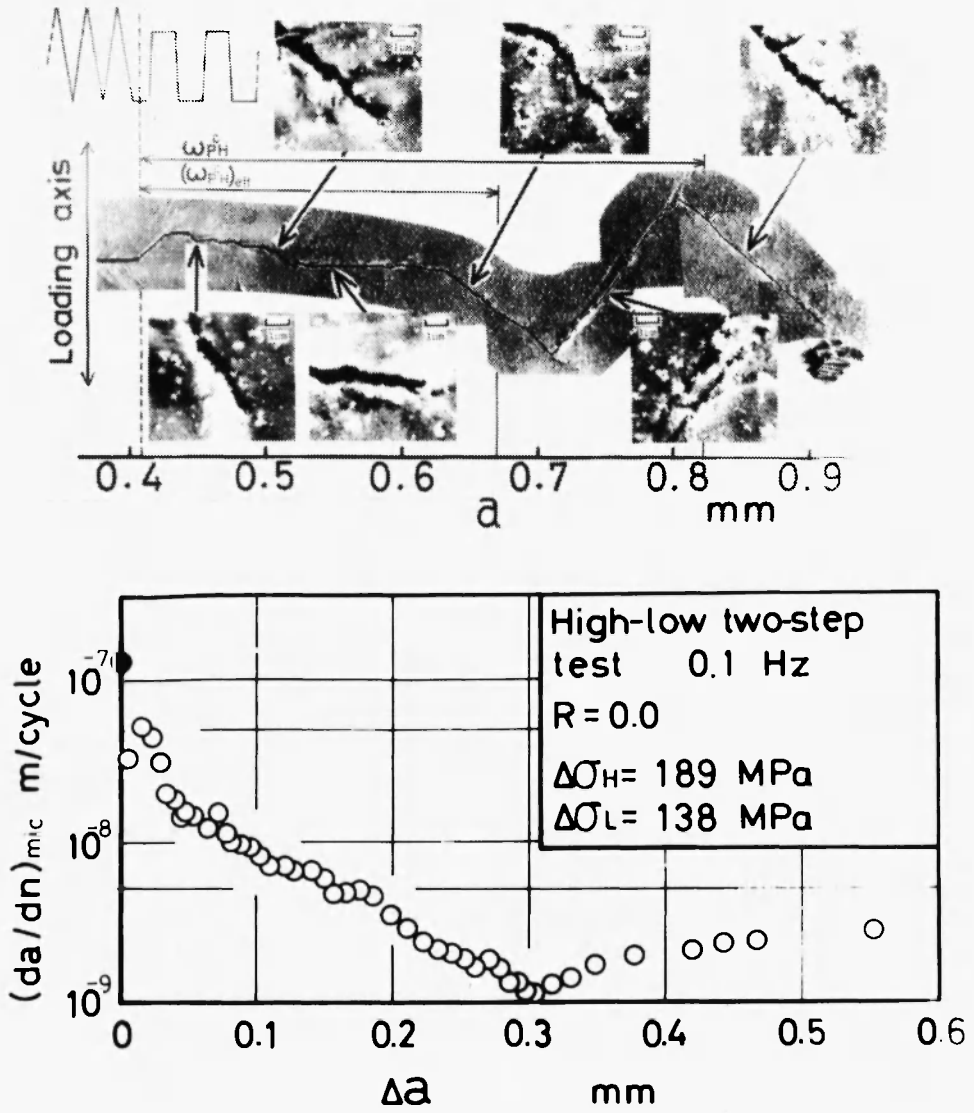

Fig.14 Macroscopic crack path and variation of growth rate with crack growth increment in Hi-Lo two step loading test.

after load reduction in Hi-Lo two step loading test [11]. Microscopic crack growth rate was calculated from the photographs as the averaged rate over the distance of 5 - 15 μm crack advance, and solid symbol corresponded to the growth rate under high level loading. It was found that the delayed retardation occurred in Hi-Lo two step loading, as widely known in such loading tests. In the figure are shown both the plane strain cyclic plastic zone size,

$\omega_{pn}^{c}=\frac{1}{2\sqrt{2}\pi}\left(\frac{\Delta K}{2\sigma_y}\right)^2$ = 0.39 mm. and the plane strain effective cyclic plastic zone size, $(\omega_{pn}^{c})_{eff}=\frac{1}{2\sqrt{2}\pi}\left(\frac{\Delta K_{eff}}{2\sigma_y}\right)^2$ = 0.24 mm corresponding to the high level loading, where σ_y is the yield stress of the material and 290 MPa. Minimum

growth rate was obtained at the crack increment between these two plastic zone sizes and then the growth rate was found to increase gradually. In this case, however, there hardly existed the correlation between crack growth rates and crack growth directions, contorary to the constant amplitude loading test, and even in the region of crack growth rate of about 10^{-8} m/cycle crack continued to grow in Mode I manner macroscopically. When the growth rate was reduced below $2x10^{-9}$ m/cycle, crack was found to grow in zigzag manner along the preferential slip directions. Thus neither the stress intensity factor nor the crack growth direction can characterize the fatigue crack growth behavior in Hi-Lo two step loadings. Figure 15 shows the relationship between crack growth rate and CTODy under Hi-Lo two step loading tests. Solid and dotted lines represent the relationship for the constant amplitude loading test of Fig.12. A considerable good agreement was found for both types of constant and variable amplitude loadings, indicating that the CTOD is a governing parameter of fatigue crack growth rates even for variable amplitude loadings.

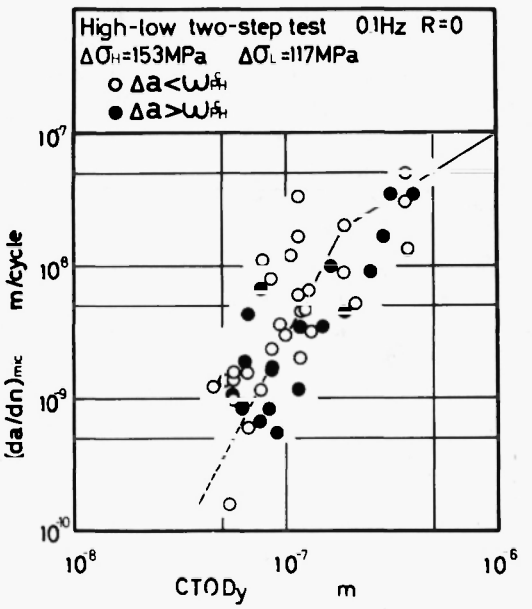

Fig.15 Relationship between crack growth rate and CTOD under Hi-Lo two step loading test.

3.4 Quantitative Analysis of Deformation Near Fatigue Crack Tip

It was tried to analize the deformation near fatigue crack tip by using the image processing technique, where two SEM images sampled at a minimum load and at a succesive maximum load were superposed and compared. Figure 16 shows the flow chart of near crack tip deformation analysis procedure. The superposition was made by corresponding magnesium oxides located in the region ahead of crack tip of two SEM images, since it was reported that little slip deformation occurred ahead the crack tip for Mode I crack[4]. Calculation of correspondences between two SEM images was carried out by using Sequential Similarity Detection Algorithm (SSDA) method. An SEM image was divided into 300 window

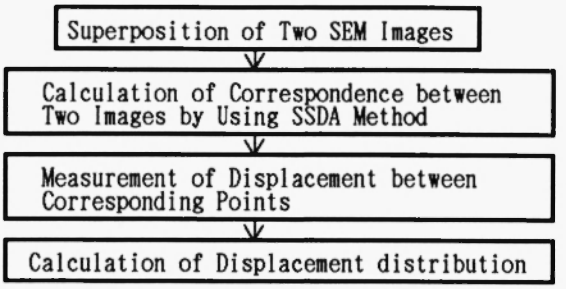

Fig.16 Flow chart of deformation analysis procedure.

areas and a corresponding area to each window area was searched on the other SEM image. Displacement is quantified by measuring a shift distance between the corresponding area. The results of deformation analysis is shown in Fig. 17. Figures 17(a) and (b) show the SEM photographs sampled at the minimum load and maximum load, respectively. In Fig. 17(c), square symbols show center of window areas in the SEM image sampled at the minimum load(Fig.17(b)) and circular symbols represent center of corresponding areas in the image sampled at the maximum load. In order to obtain continuous displacement distribution around the crack tip, spline function with two variables was fitted into the discrete displacement distribution of Fig. 17(c). The calculated results are shown in Fig.18. It was found that displacement occurred almost uniformly behind the crack tip and decreased near crack tip region, and there occurred little deformation ahead of the crack tip. Kikukawa et al. reported that deformation began to occurred at slip line passing through the crack tip for Mode I fatigue crack [4]. In this example, however, deformation was also observed to occur in the region in front of slip line, which passed through the crack tip, shown by dashed line in Figs.17 and 18. The deformation direction behind the crack tip was found to be approximately 55 degree, which coincides with the slip direction of the material.

3.5 Effect of Grain Orientation and Grain Boundary on Crack Growth Behavior

The effects of grain orientation and grain boundary on crack growth directions and rates were investigated through direct observations of growing fatigue cracks by using a randomly oriented 3% silicon iron. Figure 19 shows macroscopic crack growth path under K-increasing test, the K value of which is illustrated in lower part of the figure. Fatigue crack was found to grow within grain or along grain boundary to the direction perpendicular to the loading axis macroscopically. In microscopic sense, however, crack growth behaviors were rather complicated and different depending on grains. In Figs.20(a) - (c) are shown the details of crack path with illustration of grain boundary and corresponding microscopic crack growth rates by open circles. Solid circles and dotted line show the macroscopic crack growth rates. Further, arrows and figures given in a grain represent projected orientations of four slip directions of the grain and Schmid factors, respectively.

Firstly the effect of grain orientation will be discussed with relatively large sized grain in order to separate it from the grain boundary effect. In the grain Ⓑ, where four slip orientations are quite different with similar

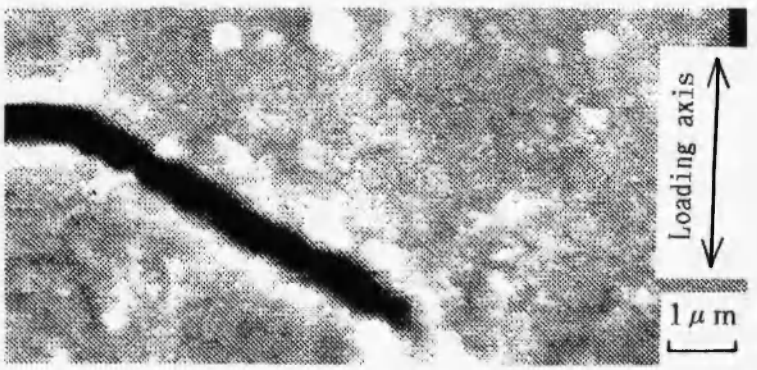

(a) SEM image sampled at the maximum load.

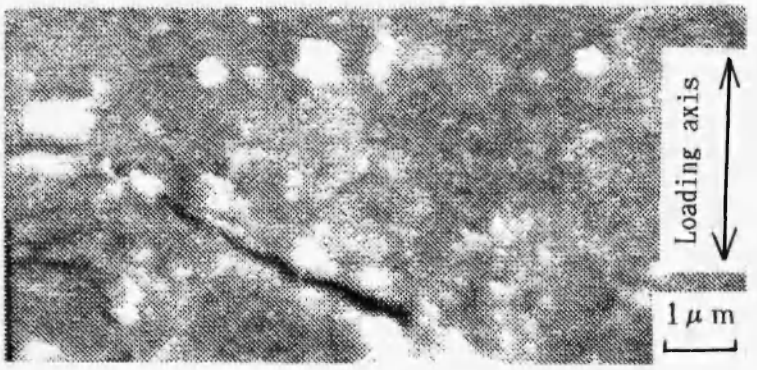

(b) SEM image sampled at the minimum load.

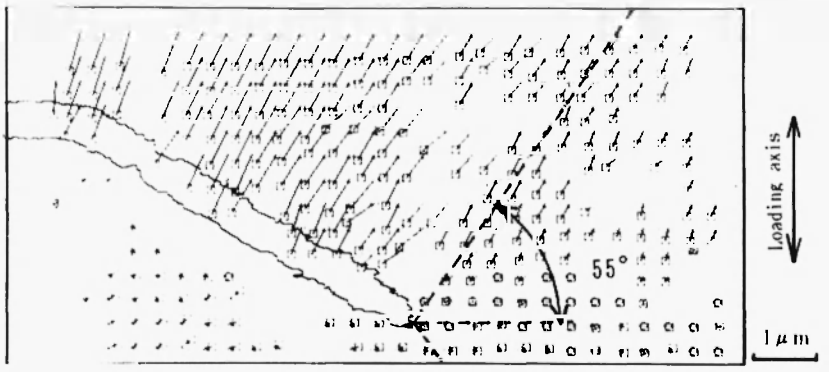

(c) Superposition of two SEM images.

Fig.17 Deformation behavior near the fatigue crack tip.

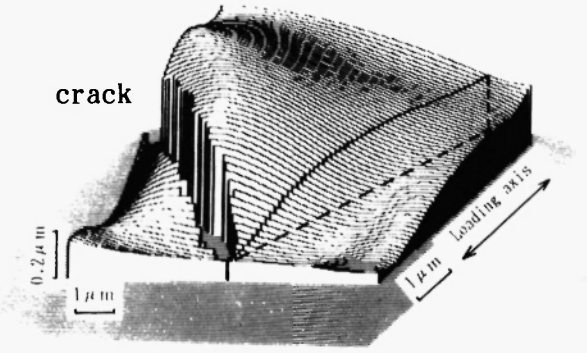

Fig.18 Displacement distribution around the fatigue crack tip.

Schmid factors, it was found that crack grew in zigzag manner along the slip directions and correspondingly had low growth rates with large scatter. Similarly in the grain Ⓓ, crack was found to refract and grow upward along the slip direction with large Schmid factor just after passing through the grain boundary. However, this crack was stopped when it approached to the grain boundary and branched crack was observed to start along the other slip direction from the refraction point. Moreover, this crack refracted again when it approached to the grain boundary. Thus grain orientations were found to strongly affect on crack growth behaviors at the relatively low stress intensity levels. However, in the grain Ⓘ, where the situation of grain orientations is similar to that of grain Ⓑ but the stress intensity level is high, nearly Mode I crack growth was observed and corresponding microscopic crack growth rates were also near to the averaged one. Similar behaviors were also found with a relatively small sized grain Ⓝ. So it may be concluded that the effect of grain orientation on crack growth behaviors seems to disappear in the high growth rate regime.

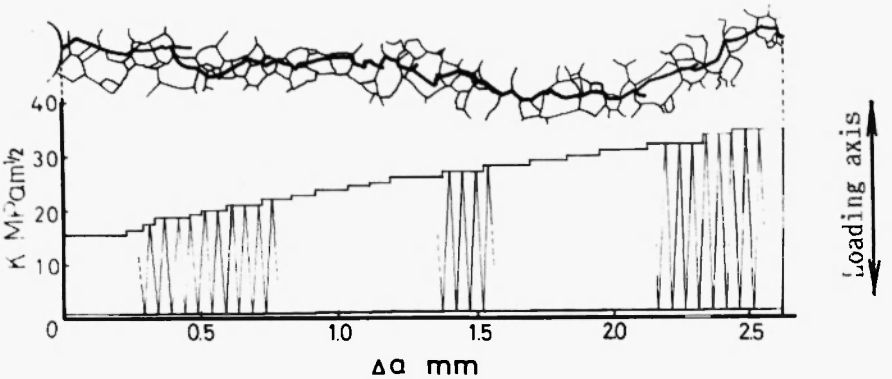

Fig.19 Schematic illustration of crack path and load history.

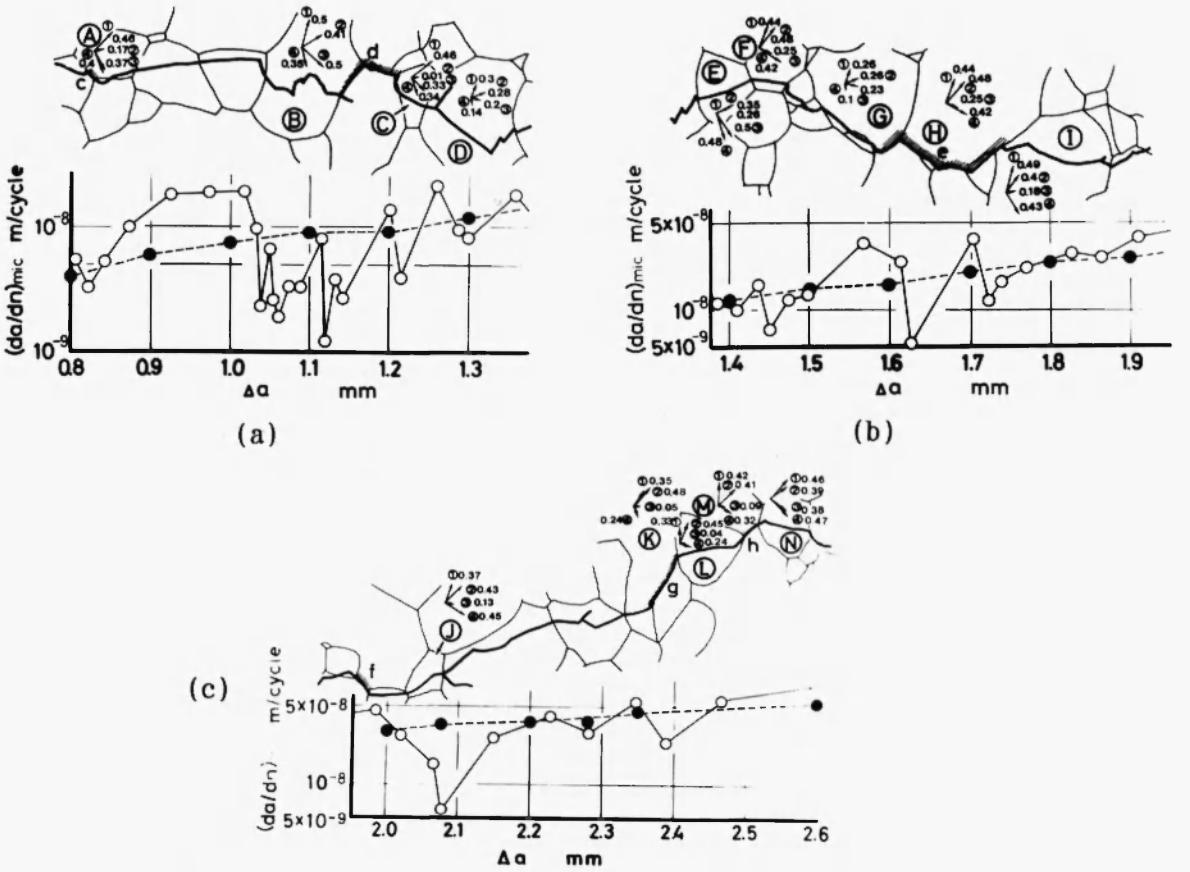

Fig.20 Microscopical crack path and variation of crack growth rate with crack increment.

The effect of grain boundary on transgranular fatigue crack growth may be understood from the following considerations; In the grain (F), although crack was intended to grow along a preferential slip direction such as direction (4), there located the grain boundary ahead of the crack in this direction which might act as an obstacle for slips, so that crack was found to grow microscopically in zigzag manner resulted in the macroscopic crack advance in the direction parallel to the grain boundary and reduced growth rates. Apart from the above mentioned discussion, if the mismatch of grain orientations between neighboring grains is small, it is supposed that crack can grow passing the grain boundary without change of growth direction, such situation being supposingly realized at the grain (A) and the neighbor, where microscopic crack growth rates were found higher than macroscopic one. So the grain boundary may have no obstructive effect on crack growth in such a case. On the other hand, at the grain boundary with the large mismatch of grain orientations crack may change the growing direction or make branch as shown in the grain (J) and the neighbor, where the obstructive effect and reduced crack growth rates were observed.

Figure 21 shows another example of fatigue crack path and distribution of microscopic crack growth rates within a grain. In this case the stress intensity level was so high that crack did grow to the perpendicular direction

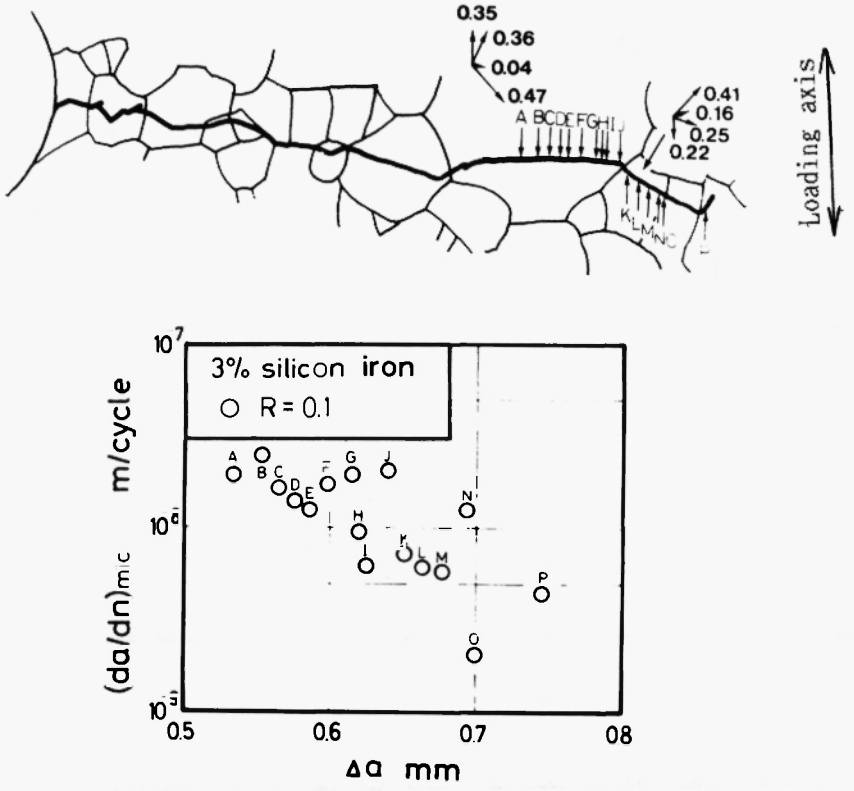

Fig.21 Crack path and variation of microscopic crack growth rate in grain.

to the loading axis. Although microscopic growth rates were found to take similar values from point Ⓐ to Ⓕ, when the crack approached to the grain boundary where the slip bands ahead of the crack tip were considered to touch the grain boundary, sudden decrease of crack growth rate was observed at points Ⓗ and Ⓘ, And when the slip bands passed the grain boundary and entered in the neighboring grain, even in the case of the crack tip still remaining in the grain, crack growth rates returned back to the former value as shown by point Ⓙ. Similar behavior was also observed in the next grain as shown by the rates of points from Ⓚ to Ⓟ. Thus it may be concluded that grain boundary has generally obstructive effects on crack growth rates.

4. CONCLUSIONS

Direct observations of growing fatigue cracks under cyclic loadings were made by the field emission type SEM equipped with a specially designed loading system on both grain oriented and randomly oriented 3% silicon irons. Fatigue crack growth mechanisms and governing parameters of growth rates were investigated by partly using a newly developed micro-computer assisted image processing techniques. Main results obtained are summarized below.

(1) Both microscopic and macroscopic fatigue crack growth directions are closely interrelated with growth rates, and the lower the growth rate is, the more macroscopic growth direction deviates from the ideal Mode I growth.

(2) A simple fatigue crack growth model at the relatively low stress intensity regime is proposed to explain the above mentioned behavior.

(3) There exists a good correlation between crack growth rate and crack tip opening displacement, CTOD, under constant amplitude loading test, and the ratio of crack growth increment to CTOD is found nearly constant and about one-tenth in the range of growth rate from 10^{-8} to $2x10^{-7}$ m/cycle. However the ratio is reduced with decrease of growth rate in the region below the growth rate of 10^{-8} m/cycle.

(4) The CTOD is found to be a governing parameter of fatigue crack growth rates even under variable amplitude loadings as well as under constant amplitude loadings.

(5) Grain orientation strongly affects fatigue crack growth behavior in the relatively low growth rate regime, and growth directions and rates are found to differ depending on grains. However, the effect of grain orientation seems to disappear in the high growth rate regime.

(6) Grain boundary is found to have obstructive effects on crack growth rates, so that fatigue crack has different growth rates even within a grain and growth rate decreases when the crack tip approaches to grain boundary.

REFFERENCES

[1] Laird, C. and Smith, G.C., Phil. Mag., Vol.7 (1962), p.847.
[2] Pelloux, R.M.N., Trans. ASM, Vol.62 (1969), p.282.
[3] Neumann, P., Acta Meta., Vol.22 (1974), p.1157.
[4] Kikukawa, M., Jono, M. and Adachi, M., ASTM STP 675, (1979), p.234
[5] Kikukawa, M., Jono, M., Iwahashi, M., Ichikawa, A. and Uesugi, N., J. Soc. Mat. Sci., Japan, Vol.31 (1982), p.669.
[6] Kikukawa, M., Jono, M. and Tanaka, K., Proc. 2nd Int. Conf. on Mech. Behavior of Materials, Boston, Special volume, (1976), p.254.
[7] Richard, C.E., Acta Meta., Vol.19 (1971), p.583.
[8] Evans, J.T., J. Mech. Phys. Solids, Vol.28 (1980), p. .
[9] Jono, M. Song, J. and Gotou, K., Trans. Japan Soc. Mech. Eng., Vol.52 (1985), p.1453.
[10] Davidson, D.L. and Lankford, J., Mat. Sci. Engng., Vol.60 (1983), p.225.
[11] Jono, M., Song, J., Gotou, K. and Yamada, S., J. Soc. Mat. Sci., Japan, Vol.35 (1986), p.918.
[12] Komai, K. and Kikuchi, J., J. Soc. Mat. Sci., Japan, Vol.34 (1985), p.648.